View metadata, citation and similar papers at core.ac.uk

brought to you by CORE

provided by E-space: Manchester Metropolitan University's Research Repository

Martínez-Periñán, E and Down, Michael and Gibaja, C and Lorenzo, E and Zamora, F and Banks, Craig (2018)*Antimonene: A Novel 2D Nanomaterial for Supercapacitor Applications.* Advanced Energy Materials, 8 (11). ISSN 1614-6832

Downloaded from: http://e-space.mmu.ac.uk/621271/

Version: Accepted Version

Publisher: Wiley

DOI: https://doi.org/10.1002/aenm.201702606

Please cite the published version

https://e-space.mmu.ac.uk

Antimonene: A novel 2D-nanomaterial for supercapacitor applications.

Emiliano Martínez-Periñán,[1,2] Michael P. Down,[2, 3] Carlos Gibaja,[4] Encarnación Lorenzo,[1] Félix Zamora,[4] and Craig E. Banks* [2, 3]

[1.] *Departamento de Química Analítica y Análisis Instrumental, Universidad Autónoma de Madrid, 28049, Madrid, Spain.*

[2.] *Faculty of Science and Engineering, Manchester Metropolitan University, Chester Street, Manchester M1 5GD, UK.*

[3.] *Manchester Fuel Cell Innovation Centre, Manchester Metropolitan University, Chester Street, Manchester M1 5GD, UK.*

[4.] *Departamento de Química Inorgánica, Universidad Autónoma de Madrid, 28049, Madrid, Spain.*

Abstract

In pursuing higher energy density, without compromising the power density of supercapacitor platforms, the application of an advanced 2D nanomaterial is utilised to maximise the performance. Antimonene, for the first time, is characterised as a material for applications in energy storage, being applied as an electrode material for supercapacitors. Antimonene is shown to significantly improve the energy storage capabilities of a carbon electrode in both cyclic voltammetry and galvanostatic charging. Demonstrating remarkable performance with a capacitance of is 1578 F g^{-1}, with a high charging current density of 14 A g^{-1}, antimonene is shown the be a highly promising material for energy storage applications. The system also demonstrates a highly competitive energy and power densities of 20 mW h kg^{-1} and 4.8 kW kg^{-1} respectively. As well as excellent charge storing capabilities, the antimonene demonstrates good cycling capabilities.

Broader Context

Supercapacitors with excellent power density and lithium ion batteries with high energy density are currently both considered novel, environmentally friendly and high-performance energy storage devices. Nevertheless, in view of numerous applications of electronic devices and hybrid electric vehicles, there has been great demand for high performance energy storage devices with both higher energy density and power density; a device that provides both long lasting energy storage with short charging times. A simple solution to this is a device, which utilises a supercapacitor arrangement in parallel, providing a simple fast charging solution, with the high energy storage capacity of the parallel battery. Typical arrangement of such systems utilise activated carbon as supercapacitor electrode materials, which, although affordable, demonstrates relatively low conductivity, low capacity and poor stability in lifecycle testing. As a result, advanced nanomaterials have developed significant interest in the energy storage fields. A highly novel nanomaterial is presented here for the first time as an electrode material for energy storage architectures. Antimonene, a 2D nanomaterial of antimony, is, for the first time characterised as a material for energy storage applications.

Introduction

The increasing development and demand of renewable and sustainable energy sources have required the development of sustainable energy storage technologies in order to satisfy the increasing demand for *green* energy[1,2]. Because of their high power density, competitive energy density, good operational safety, long cycling life, and minimum charge separation compared to alternative energy storage platforms, electrochemical double-layer capacitors (EDLC) or supercapacitors have been considered an energy storage platform with significant potential. Supercapacitors have been extensively explored and are recognized as promising devices for energy applications from high-power electronics down to fast charging personal electronic devices, from electric vehicles and hybrid electric vehicles down to mobile phones[3-5]

Advancements in nanomaterials and nanotechonology are playing a key role in bringing these devices toward practical applications and improvement in device performance, scale and compatibility. Increasingly more attention has been paid to the development of nanomaterials, which are expected to allow electrodes development with major storage devices[6]. 2D nanomaterials have spiked interest due to their high specific surface area, a material property that can significantly contribute to a high double-layer capacitance. Furthermore, 2D nanomaterials have reactive basal planes and edges that can provide electrochemical performance enhancement such as pseudo-capacitance[7]. After graphene's successful application in different energy storage devices[8-11], new 2D inorganic nanomaterials have been developed[12], most with similar crystalline structures[13]. Such 2D nanomaterials have shown great promise as electrode materials when layered onto the electrodes in electrochemical energy-storage devices in which efficient intercalation of ions play an important role[14,15]. They involve van der Waals interactions between adjacent sheets with strong covalent bonding within each sheet. There are very good reasons for the exploration of these nanomaterials, which is that monolayer materials show increased bandgap and tunable electronic, optical, catalytic, and electrochemical properties[16]. Such materials span the entire range of electronic structures, from insulator to metal, and display intriguing properties[17]. Recently some studies are being carried out successfully for the application of graphene-like layered material with electrochemical applications like transition metal dichalcogenides[18]. Even so some of this new 2D-nanomaterial are showing desirable performance in supercapacitors applications like, 2Dh-boron nitride[19], metal oxides[20-22], metal carbides[23] and metal dichalcogenides[24].

In recent years, a new family of compounds similar to graphene, based on anisotropic layered elemental materials, are attracting the attention of the scientific community. These materials, ideally, consist of one atom thick type two dimensions structure; each atom is covalently bonded with adjacent atoms to form a puckered honeycomb structure. For example, phosphorene, from an allotrope of phosphorous,

black-phosphorus[25], is worthwhile to be mentioned because of the interesting properties with applications in optoelectronics and electronics[26,27] and in energy storage devices[28-31]. The success of phosphorene has carried on the attention to the rest of fifth main group of elements[16], and new materials such as Arsenene, Antimonene, and Bismuthene have been predicted with interesting properties[32-34], and even so some of them have been isolated[35,36]. Antimonene is considered a material of great interest for applications in electrochemistry and has been also isolated from its layered allotrope form. Firstly it has been isolated by mechanical exfoliation[37] and then by liquid-phase exfoliation[38].

In this work, we have focused our attention on the electrochemical capacitive performance of antimonene flakes. There are not any electrochemical study on this new 2D-nanomaterial in this form, and we have demonstrated the successful application of it as a supercapacitor, obtaining highly competitive specific capacitances values, laying the basic aspects of a new research line on energy storage devices with the use of antimonene.

Results and discussion

Modified SPE characterization

Modified SPEs have been characterized by SEM and Raman spectroscopy in order to confirm the proper modification of the electrodes with the 2D-nanomaterial. SEM images Figures 1 A, B and C clearly show the deposit of small particles (flakes) of antimonene compare with the bare SPE SEM image fig 1 D. As can be observed in SEM images, shown in Figure 1, antimonene form flakes with lateral dimension around 200-400 nm. This is a typical antimonene morphology, agreeing well with that described in the literature describing the synthesis[38]. The atomic composition of the flakes is antimony, Sb, as can be determined by EDX spectrum (Figure ESI 1 and Table ESI 1). The presence of these nanoflakes

Raman spectroscopy also confirm the presence of antimonene over the modified SPEs surface (Figures 2A and 2B). In addition to the Raman bands associated with carbon, which constitutes the base of the SPE, two Raman bands, associated with the antimony (Sb) A_{1g} and E_g vibrational modes at 149.8 cm^{-1} and mode at 110 cm^{-1} respectively, were detected. The intensity of these bands increase when higher amounts of antimonene are drop-casted over the SPE surface, which indicates at the same time higher antimony deposition and even that the thickness of these nanostructures could increase. This fact could be related with the decrease of capacitance observed in the next showed results, when higher amounts of antimonene are drop-casted over the SPE, being consequence of less electroactive surface of the 2d-nanomaterial when higher nanostructures are deposited or the stack of the small few layers antimonene flakes occurs.

As a new 2D-nanomaterial that has little known regarding its physicochemical and capacitive properties for electrochemical applications, antimonene enhanced SPE's, A-SPEs, electrochemical behavior with a redox probe has been studied, using cyclic voltammetric responses in 1 mM $Ru(NH_3)_6^{3+}$ in 0.1 M KCl (figure S2 A, B and C and table S2). No important variation of electron transfer rate constant was observed, which indicates no difference in the electrochemical process. However, a slight increase in the redox peak intensity occurs as a consequence of the increase of electrochemical active area generated by the nanomaterial in the electrode surface. It becomes clear from these results that few layer antimonene flakes are behaving as a good conducting material, with a high heterogeneous electron transfer rate, an order of magnitude higher than that of the carbon ink used in the typical SPE. This result was expected, as previously reported in the literature, which shows the semi-metallic behavior of antimonene, proving that two or more layers of antimonene nanostructures is a conductive material[37].

Exploring antimonene as a capacitive material

We first consider the cyclic voltammetric responses of the bare SPE utilizing a two-electrode system in 0.5 M H_2SO_4 at different scan rates, which provides a benchmark, after which we analyzed the response exhibited upon drop casting of antimonene amounts ranging from 1.8 to 36 ng (Figure 3 A, B and C). It can be clearly observe the increase of capacitive current when small amounts of antimonene are drop-casted onto the SPE. Even so, a redox process is observed at formal potential 0.0 V, which could be ascribed to the oxidation and reduction of antimonene, as a consequence of a faradaic process which also contributes significantly to the capacitance increase. With the clear presence of faradaic electrochemistry, cyclic voltammetry measurements with a 3 electrode configuration (antimonene/SPE as working electrode, saturated calomel as reference electrode, and a platinum wire as counter) were carried on acid media (0.5 M H_2SO_4) (Figure ESI3). As can be observed in the voltammogram an anodic stripping peak is observed at 0.08 V, ascribed to the oxidation of Sb atoms to Sb (III) cathions. This peak increase during the voltammetry scans applied, until it stabilized (fifth scan). No clear reversible reduction peak are observed in the voltammogram, unless we consider Sb (III) cation reduction occurs at the same potential of solvent discharge, regenerating the Sb atoms in the antimonene structure previously oxidized, keeping the nanomaterial unaltered.

The capacitance of the working electrode, C_{WE}, was calculated from the corresponding voltammograms, as shown in Figure 3, using the following equation:

$$C_{we} = \frac{\int_{V_1}^{V_2} I(V)dV}{2 \cdot \Delta V \cdot v \cdot m} \qquad (1)$$

where C_{we} is the specific capacitance exhibited by the working electrode in faradays per gram *(F/g),* $\int I(V)dV$ is the area under the intensity current function between V_2 and V_1 potentials in coulombs (C), essentially a measure of the charge stored by the capacitor device. ΔV is the potential difference between *V2* and *V1* in volts (V), *v* is the voltammograms scan rate in volts per second (V/s) and *m* is the material (antimonene) mass in grams. The determined capacitance values are showed in table 1 and Figure 3D. Huge capacitance values are obtained, being that in the best configuration of around 8500 F/g. This huge value determined are the consequence of the combination of two factors, on the first hand the increase of electrochemical active area and the consequence increase of the electrochemical double layer over the electrode surface. On the other hand, these huge values are a consequence of the faradaic process describe, increasing the area under the current curves because of the redox peak.

In order to have more realistic capacitance values, galvanostatic charge/discharge study was performed using a two-electrode approach to compliment the setup utilized for supercapacitors within the field. Figure 4A illustrates the charge/discharge profiles obtained for bare SPE, and antimonene modified SPE with increasing amounts of the 2d-nanomaterial. The results clearly show that *dV/dt* decrease, which is a consequence of the capacitance increase when SPE are modified with the 2d-nanomaterial. Capacitances values and specific capacitance values are shown in table II and III respectively. These values are lower than the obtained by CV, but we consider it more realistic values, and no faradaic process are involved in that case. The specific capacitance in the best configuration 3.6 ng Antimonene/SPE at a current of 14 A g^{-1} is 1578 F g^{-1} (Figure 4C). This high value is competitive with other 2D-nanomaterial that are being proving as supercapacitor material[19,39-41], and with other types of material use in supercapacitors[42-46]. As can be see (Figure 4B) the absolute capacitance values increase with the amount of antimonene deposited onto the SPE surface until we modified with 18.0 ng antimonene. From that 2D-nanomaterial mass, the capacitance decrease, which could be a consequence of the nanomaterial agglomeration or stacking, decreasing the electroactive surface area.

For supercapacitors, cycling stability is also a very important parameter. Therefore, the charge-discharge stability was studied over 10000 galvanostatic cycles applying a specific current of 14 Ag^{-1} on a 36 ng antimonene/SPE (Figure 4D). The capacitance retention values demonstrate that after an initial drop to 65% the successive cycles retain the capacitance between 65-63% of the initial capacitance over the entire range of cycles, showing the same capacitance between the scan 800 to the 10000. This result proved that after an initial stabilization the capacitance keep constant at least more than 9000 charge-discharge cycles, the maximum number of cycles that has been experimentally study on this work. It is likely that the decrease in the first 1000 cycles can be attributed to some of the drop cast antimonene being liberated from the electrode surface with charge cycling.

Typically, a supercapacitors exhibit a low energy density, *E,* and a high power density, *P*, the values of which are calculated using $E=I\,(dV)(dt)/2m$ and $P=(I(dV))/2m$ respectively, where m is the mass of the antimonene residing upon the surface of the SPE (i.e. 1.8 ng), in this case the values correspond to 0.02 W h kg^{-1} and 4800 W kg^{-1} respectively. These values are indicative of a high power supercapacitor and a similar.

Experimental

All chemicals utilized were of analytical grade and were used as received from Sigma-Aldrich without any further purification. All solutions were prepared with deionized water of resistivity not less than 18.2 MΩ·cm and (when necessary) were vigorously degassed prior to electrochemical measurements with high purity, oxygen free nitrogen.

Single or few layers antimonene suspension were prepared according to the describe method by Gibaja *et al.* [38] Briefly the method consist on applied sonication to antimony crystals in a 4:1 isopropanol/water mixture without any surfactant, generating a very stable suspension of micrometer large few layers antimonene over weeks, even under ambient conditions.

The working electrodes used were screen-printed graphite electrodes (SPEs). The SPEs, which have a 3 mm diameter working electrode, were fabricated in-house with appropriate stencil designs using a microDEK 1760RS screen-printing machine (DEK, Weymouth, UK). The SPE design has been previously reported[47]. For the case of each fabricated electrode, First a graphite ink formulation (Product Code: C2000802P2; Gwent Electronic Materials Ltd, UK), which is utilized for the efficient connection of all three electrodes and as the ink material for both the working and counter electrodes, was screen-printed onto a polyester (Autostat, 250 mm thickness) Flexible film. After curing the screen-printed graphite layer in a fan oven at 60 ºC for 30 minutes. Finally, a dielectric paste (Product Code: D2070423D5; Gwent Electronic Materials Ltd, UK) was then screen-printed onto the polyester substrate to cover the connections and define the active electrode areas, including that of the working electrode (3 mm diameter). After curing at 60 ºC for 30 minutes the SPEs are ready to be used.

Antimonene modified electrodes were prepared by drop-casting aliquots of the 0.02 g/L antimonene 4:1 isopropanol/water suspension onto the required working electrode with a micropipette. After few minutes, the solvent completely evaporated (at ambient temperature) and the modified electrodes utilised without further modification. All electrochemical measurements were performed with an Autolab TYPE III (Autolab, The Netherlands). It is noted that the charge-discharge curves and cyclic voltammetry for capacitances measures were obtained using a two-electrode configuration and the cyclic voltammetric (CV) studies, using Ru(NH3)63+ and H2SO4 to characterize the electrochemical behavior of antimonene in acid media were carried out utilizing a three-electrode system, where a platinum wire and saturated calomel electrode (SCE) were used as counter and reference electrodes respectively.

Scanning electron microscopy (SEM) images and surface element analysis were carried on using a JEOL JSM- 5600LV model equipped with an energy-dispersive X-ray (EDX) microanalysis package.

Raman spectroscopy analysis of antimonene modified SPE surfaces was done using a 'Renishaw InVia' spectrometer with a confocal microscope (x50 objective) spectrometer with an argon laser (514.3 nm excitation) at a very low laser power level (1.2 mW) to avoid any heating effects. Spectra were obtained using a 10 second exposure time for 3 accumulations.

Conclusions

Antimonene, for the first time, is characterised as a material for applications in energy storage, being applied as an electrode material for supercapacitors. It is shown to significantly improve the energy storage capabilities of a carbon electrode substrate in both cyclic voltammetry and galvanostatic charging. Demonstrating remarkable performance with a capacitance of is 1578 F g^{-1} with a high charging current density of 14 A g^{-1} antimonene is shown the be a promising material for energy storage applications. The antimonene enhanced electrodes demonstrate a pseudo-capacitive faradaic voltammetric response, which is shown to enhance the electrochemical capacitive performance of the electrode materials. The presence of the antimonene is shown to significantly increase the capacitive performance of the supercapacitors when compare to a device with bare graphitic electrodes. Quantities of antimonene as little as 1.8 ng of material are shown to significantly improve the capacitive performance of the system. The system also demonstrates a highly competitive energy and power densities of 20 mW h kg^{-1} and 4.8 kW kg^{-1} respectively. As well as excellent charge storing capabilities, the antimonene demonstrates good cycling capabilities over 1000 cycles until the drop cast material is liberated from the substrate.

Acknowledgements

Funding from the Engineering and Physical Sciences Research Council (Reference: EP/N001877/1), British Council Institutional Grant Link (No. 172726574) and the Russian Foundation for Fundamental Research (No. 16-03-00846) is acknowledged. E. Martínez-Periñán acknowledges funding from Comunidad de Madrid (NANOAVANSENS Program) for financial support.

References

1 Abruña, H. D. Energy in the Age of Sustainability. *Journal of Chemical Education* **90**, 1411-1413, doi:10.1021/ed400673m (2013).

2 Chow, J., Kopp, R. J. & Portney, P. R. Energy Resources and Global Development. *Science* **302**, 1528-1531, doi:10.1126/science.1091939 (2003).

3 Kötz, R. & Carlen, M. Principles and applications of electrochemical capacitors. *Electrochimica Acta* **45**, 2483-2498, doi:http://doi.org/10.1016/S0013-4686(00)00354-6 (2000).

4 González, A., Goikolea, E., Barrena, J. A. & Mysyk, R. Review on supercapacitors: Technologies and materials. *Renewable and Sustainable Energy Reviews* **58**, 1189-1206, doi:http://doi.org/10.1016/j.rser.2015.12.249 (2016).

5 Zhang, L. L. & Zhao, X. S. Carbon-based materials as supercapacitor electrodes. *Chemical Society Reviews* **38**, 2520-2531, doi:10.1039/b813846j (2009).

6 Thangavelu, P. & Jong-Beom, B. Graphene based 2D-materials for supercapacitors. *2D Materials* **2**, 032002 (2015).

7 Mendoza-Sánchez, B. & Gogotsi, Y. Synthesis of Two-Dimensional Materials for Capacitive Energy Storage. *Advanced Materials* **28**, 6104-6135, doi:10.1002/adma.201506133 (2016).

8 Xiong, P., Zhu, J., Zhang, L. & Wang, X. Recent advances in graphene-based hybrid nanostructures for electrochemical energy storage. *Nanoscale Horizons* **1**, 340-374, doi:10.1039/c5nh00134j (2016).

9 El-Kady, M. F., Shao, Y. & Kaner, R. B. Graphene for batteries, supercapacitors and beyond. *Nature Reviews Materials* **1**, 16033, doi:10.1038/natrevmats.2016.33 (2016).

10 Wen, L., Li, F. & Cheng, H.-M. Carbon Nanotubes and Graphene for Flexible Electrochemical Energy Storage: from Materials to Devices. *Advanced Materials* **28**, 4306-4337, doi:10.1002/adma.201504225 (2016).

11 Ji, J. *et al.* Advanced Graphene-Based Binder-Free Electrodes for High-Performance Energy Storage. *Advanced Materials* **27**, 5264-5279, doi:10.1002/adma.201501115 (2015).

12 Tan, C. *et al.* Recent Advances in Ultrathin Two-Dimensional Nanomaterials. *Chemical Reviews*, doi:10.1021/acs.chemrev.6b00558 (2017).

13 Tang, Q., Zhou, Z. & Chen, Z. Innovation and discovery of graphene-like materials *via* density-functional theory computations. *Wiley Interdisciplinary Reviews: Computational Molecular Science* **5**, 360-379, doi:10.1002/wcms.1224 (2015).

14 Yoo, E. *et al.* Large Reversible Li Storage of Graphene Nanosheet Families for Use in Rechargeable Lithium Ion Batteries. *Nano Letters* **8**, 2277-2282, doi:10.1021/nl800957b (2008).

15 Mai, L. *et al.* Fast Ionic Diffusion-Enabled Nanoflake Electrode by Spontaneous Electrochemical Pre-Intercalation for High-Performance Supercapacitor. *Scientific Reports* **3**, 1718, doi:10.1038/srep01718 (2013).

16 Pumera, M. & Sofer, Z. 2D Monoelemental Arsenene, Antimonene, and Bismuthene: Beyond Black Phosphorus. *Advanced Materials*, 1605299-n/a, doi:10.1002/adma.201605299 (2017).

17 Xu, M., Liang, T., Shi, M. & Chen, H. Graphene-Like Two-Dimensional Materials. *Chemical Reviews* **113**, 3766-3798, doi:10.1021/cr300263a (2013).

18 Rowley-Neale, S. J. *et al.* 2D molybdenum disulphide (2D-MoS2) modified electrodes explored towards the oxygen reduction reaction. *Nanoscale* **8**, 14767-14777, doi:10.1039/c6nr04073j (2016).

19 Khan, A. F., Down, M. P., Smith, G. C., Foster, C. W. & Banks, C. E. Surfactant-exfoliated 2D hexagonal boron nitride (2D-hBN): role of surfactant upon the electrochemical reduction of oxygen and capacitance applications. *Journal of Materials Chemistry A* **5**, 4103-4113, doi:10.1039/C6TA09999H (2017).

20 Sugimoto, W., Iwata, H., Yasunaga, Y., Murakami, Y. & Takasu, Y. Preparation of Ruthenic Acid Nanosheets and Utilization of Its Interlayer Surface for Electrochemical Energy Storage. *Angewandte Chemie International Edition* **42**, 4092-4096, doi:10.1002/anie.200351691 (2003).

21 Kai, K. *et al.* Electrochemical characterization of single-layer MnO2 nanosheets as a high-capacitance pseudocapacitor electrode. *Journal of Materials Chemistry* **22**, 14691-14695, doi:10.1039/c2jm31080e (2012).

22 Xiao, X. *et al.* Scalable salt-templated synthesis of two-dimensional transition metal oxides. *Nature Communications* **7**, 11296, doi:10.1038/ncomms11296

https://www.nature.com/articles/ncomms11296#supplementary-information (2016).

23 Li, J. *et al.* Achieving High Pseudocapacitance of 2D Titanium Carbide (MXene) by Cation Intercalation and Surface Modification. *Advanced Energy Materials*, 1602725-n/a, doi:10.1002/aenm.201602725 (2017).

24 Acerce, M., Voiry, D. & Chhowalla, M. Metallic 1T phase MoS2 nanosheets as supercapacitor electrode materials. *Nat Nano* **10**, 313-318, doi:10.1038/nnano.2015.40

http://www.nature.com/nnano/journal/v10/n4/abs/nnano.2015.40.html#supplementary-information (2015).

25 Wang, L., Sofer, Z. & Pumera, M. Voltammetry of Layered Black Phosphorus: Electrochemistry of Multilayer Phosphorene. *ChemElectroChem* **2**, 324-327, doi:10.1002/celc.201402363 (2015).

26 Li, L. *et al.* Black phosphorus field-effect transistors. *Nat Nano* **9**, 372-377, doi:10.1038/nnano.2014.35

http://www.nature.com/nnano/journal/v9/n5/abs/nnano.2014.35.html#supplementary-information (2014).
27 Buscema, M. *et al.* Fast and Broadband Photoresponse of Few-Layer Black Phosphorus Field-Effect Transistors. *Nano Letters* **14**, 3347-3352, doi:10.1021/nl5008085 (2014).
28 Hao, C. *et al.* Flexible All-Solid-State Supercapacitors based on Liquid-Exfoliated Black-Phosphorus Nanoflakes. *Advanced Materials* **28**, 3194-3201, doi:10.1002/adma.201505730 (2016).
29 Park, C. M. & Sohn, H. J. Black Phosphorus and its Composite for Lithium Rechargeable Batteries. *Advanced Materials* **19**, 2465-2468, doi:10.1002/adma.200602592 (2007).
30 Sun, J. *et al.* Formation of Stable Phosphorus–Carbon Bond for Enhanced Performance in Black Phosphorus Nanoparticle–Graphite Composite Battery Anodes. *Nano Letters* **14**, 4573-4580, doi:10.1021/nl501617j (2014).
31 Song, J. *et al.* Chemically Bonded Phosphorus/Graphene Hybrid as a High Performance Anode for Sodium-Ion Batteries. *Nano Letters* **14**, 6329-6335, doi:10.1021/nl502759z (2014).
32 Zhang, S. *et al.* Semiconducting Group 15 Monolayers: A Broad Range of Band Gaps and High Carrier Mobilities. *Angewandte Chemie International Edition* **55**, 1666-1669, doi:10.1002/anie.201507568 (2016).
33 Kamal, C. & Ezawa, M. Arsenene: Two-dimensional buckled and puckered honeycomb arsenic systems. *Physical Review B* **91**, 085423 (2015).
34 Zhu, Z., Guan, J. & Tománek, D. Strain-induced metal-semiconductor transition in monolayers and bilayers of gray arsenic: A computational study. *Physical Review B* **91**, 161404 (2015).
35 Walker, E. S. *et al.* Large-Area Dry Transfer of Single-Crystalline Epitaxial Bismuth Thin Films. *Nano Letters* **16**, 6931-6938, doi:10.1021/acs.nanolett.6b02931 (2016).
36 Wu, X. *et al.* Epitaxial Growth and Air-Stability of Monolayer Antimonene on PdTe2. *Advanced Materials* **29**, 1605407-n/a, doi:10.1002/adma.201605407 (2017).
37 Ares, P. *et al.* Antimonene: Mechanical Isolation of Highly Stable Antimonene under Ambient Conditions (Adv. Mater. 30/2016). *Advanced Materials* **28**, 6515-6515, doi:10.1002/adma.201670209 (2016).
38 Gibaja, C. *et al.* Few-Layer Antimonene by Liquid-Phase Exfoliation. *Angewandte Chemie International Edition* **55**, 14345-14349, doi:10.1002/anie.201605298 (2016).
39 Chen, H. *et al.* Eco-friendly synthesis of few-layer graphene with high surface area under low temperature for supercapacitors. *Electrochimica Acta* **206**, 10-16, doi:http://dx.doi.org/10.1016/j.electacta.2016.04.141 (2016).
40 Gao, S. *et al.* Ultrahigh Energy Density Realized by a Single-Layer β-Co(OH)2 All-Solid-State Asymmetric Supercapacitor. *Angewandte Chemie International Edition* **53**, 12789-12793, doi:10.1002/anie.201407836 (2014).
41 Li, Z., Zhang, W., Sun, C., Feng, Z. & Yang, B. Controlled synthesis of Ni(OH)2/graphene composites and their transformation to NiO/graphene for energy storage. *Electrochimica Acta* **212**, 390-398, doi:http://dx.doi.org/10.1016/j.electacta.2016.07.020 (2016).
42 Li, Y. *et al.* Ultra-fine CuO Nanoparticles Embedded in Three-dimensional Graphene Network Nano-structure for High-performance Flexible Supercapacitors. *Electrochimica Acta* **234**, 63-70, doi:http://dx.doi.org/10.1016/j.electacta.2017.02.167 (2017).
43 Wang, X. *et al.* High capacitance and rate capability of Ni3S2@CdS core-shell nanostructures supercapacitor. *Journal of Materials Chemistry A*, doi:10.1039/c7ta00593h (2017).
44 Roberts, M. E., Wheeler, D. R., McKenzie, B. B. & Bunker, B. C. High specific capacitance conducting polymer supercapacitor electrodes based on poly(tris(thiophenylphenyl)amine). *Journal of Materials Chemistry* **19**, 6977-6979, doi:10.1039/b916666a (2009).
45 Xu, P. *et al.* Preparation of porous cadmium sulphide on nickel foam: a novel electrode material with excellent supercapacitor performance. *Journal of Materials Chemistry A* **4**, 4920-4928, doi:10.1039/c5ta09740a (2016).
46 Qian, L. *et al.* High specific capacitance of CuS nanotubes in redox active polysulfide electrolyte. *RSC Advances* **3**, 1703-1708, doi:10.1039/c2ra22257d (2013).
47 Randviir, E. P., Brownson, D. A. C., Metters, J. P., Kadara, R. O. & Banks, C. E. The fabrication, characterisation and electrochemical investigation of screen-printed graphene electrodes. *Physical Chemistry Chemical Physics* **16**, 4598-4611, doi:10.1039/c3cp55435j (2014).
48 Wu, Z.-S. *et al.* Three-Dimensional Nitrogen and Boron Co-doped Graphene for High-Performance All-Solid-State Supercapacitors. *Advanced Materials* **24**, 5130-5135, doi:10.1002/adma.201201948 (2012).
49 Mendoza-Sánchez, B., Rasche, B., Nicolosi, V. & Grant, P. S. Scaleable ultra-thin and high power density graphene electrochemical capacitor electrodes manufactured by aqueous exfoliation and spray deposition. *Carbon* **52**, 337-346, doi:http://dx.doi.org/10.1016/j.carbon.2012.09.035 (2013).
50 Lin, J. *et al.* 3-Dimensional Graphene Carbon Nanotube Carpet-Based Microsupercapacitors with High Electrochemical Performance. *Nano Letters* **13**, 72-78, doi:10.1021/nl3034976 (2013).
51 Singu, B. S. & Yoon, K. R. Synthesis and characterization of MnO2-decorated graphene for supercapacitors. *Electrochimica Acta* **231**, 749-758, doi:http://dx.doi.org/10.1016/j.electacta.2017.01.182 (2017).
52 Zou, Y., Kinloch, I. A. & Dryfe, R. A. W. Nitrogen-doped and crumpled graphene sheets with improved supercapacitance. *Journal of Materials Chemistry A* **2**, 19495-19499, doi:10.1039/c4ta04076g (2014).
53 Li, S. *et al.* Ultrathin Nitrogen-Enriched Hybrid Carbon Nanosheets for Supercapacitors with Ultrahigh Rate Performance and High Energy Density. *ChemElectroChem* **4**, 369-375, doi:10.1002/celc.201600614 (2017).
54 Deng, L. *et al.* RuO2/graphene hybrid material for high performance electrochemical capacitor. *Journal of Power Sources* **248**, 407-415, doi:http://dx.doi.org/10.1016/j.jpowsour.2013.09.081 (2014).

55 Li, Z., Wu, L., Wang, L., Gu, A. & Zhou, Q. Nickel cobalt sulfide nanosheets uniformly anchored on porous graphitic carbon nitride for supercapacitors with high cycling performance. *Electrochimica Acta* **231**, 617-625, doi:http://dx.doi.org/10.1016/j.electacta.2017.02.087 (2017).

56 Lukatskaya, M. R. *et al.* Cation Intercalation and High Volumetric Capacitance of Two-Dimensional Titanium Carbide. *Science* **341**, 1502 (2013).

Figure 1. SEM images at different magnifications of (A) (B) (C) 36 ng antimonene/SPE and (D) bare SPE.

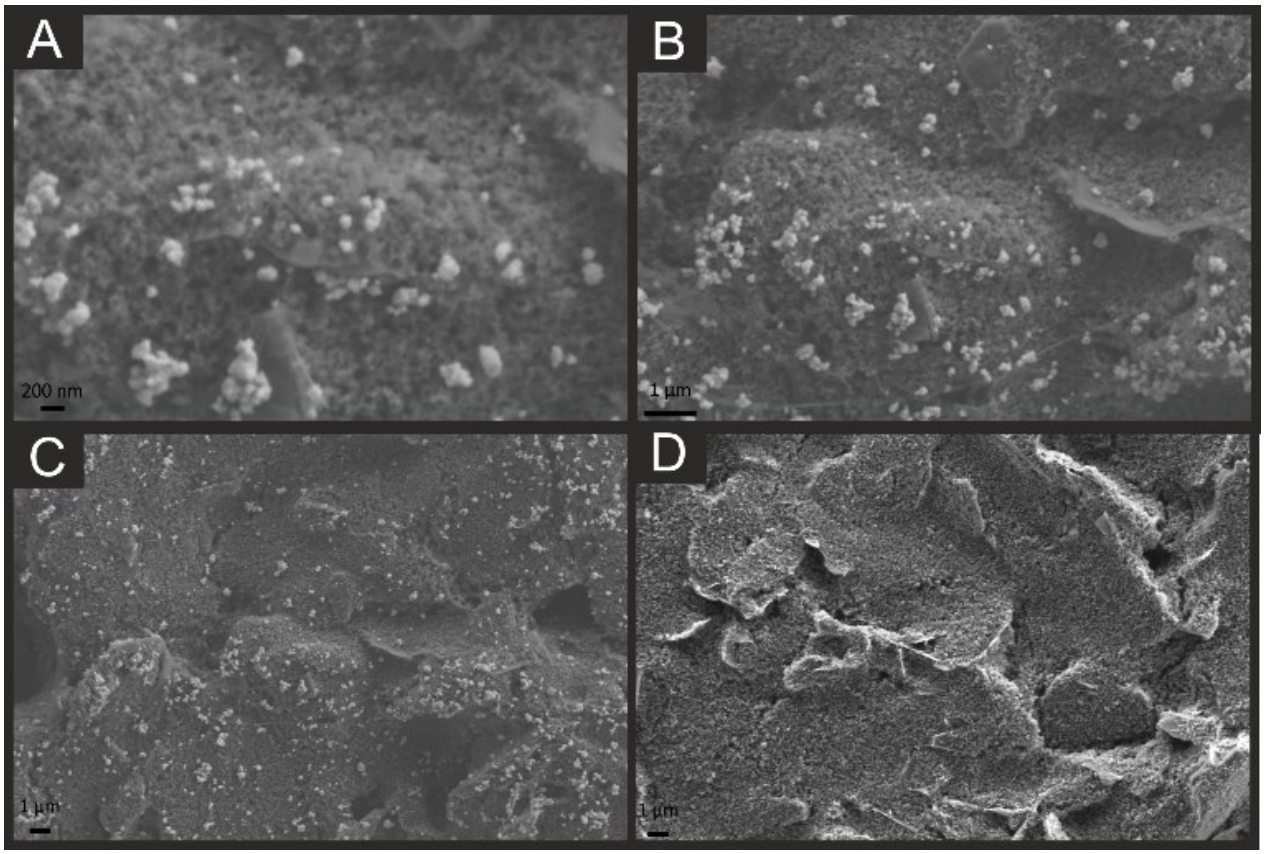

Figure 2. (A) and (B) Raman spectra of bare SPE and modified antimonene/SPE with different amounts of antimonene.

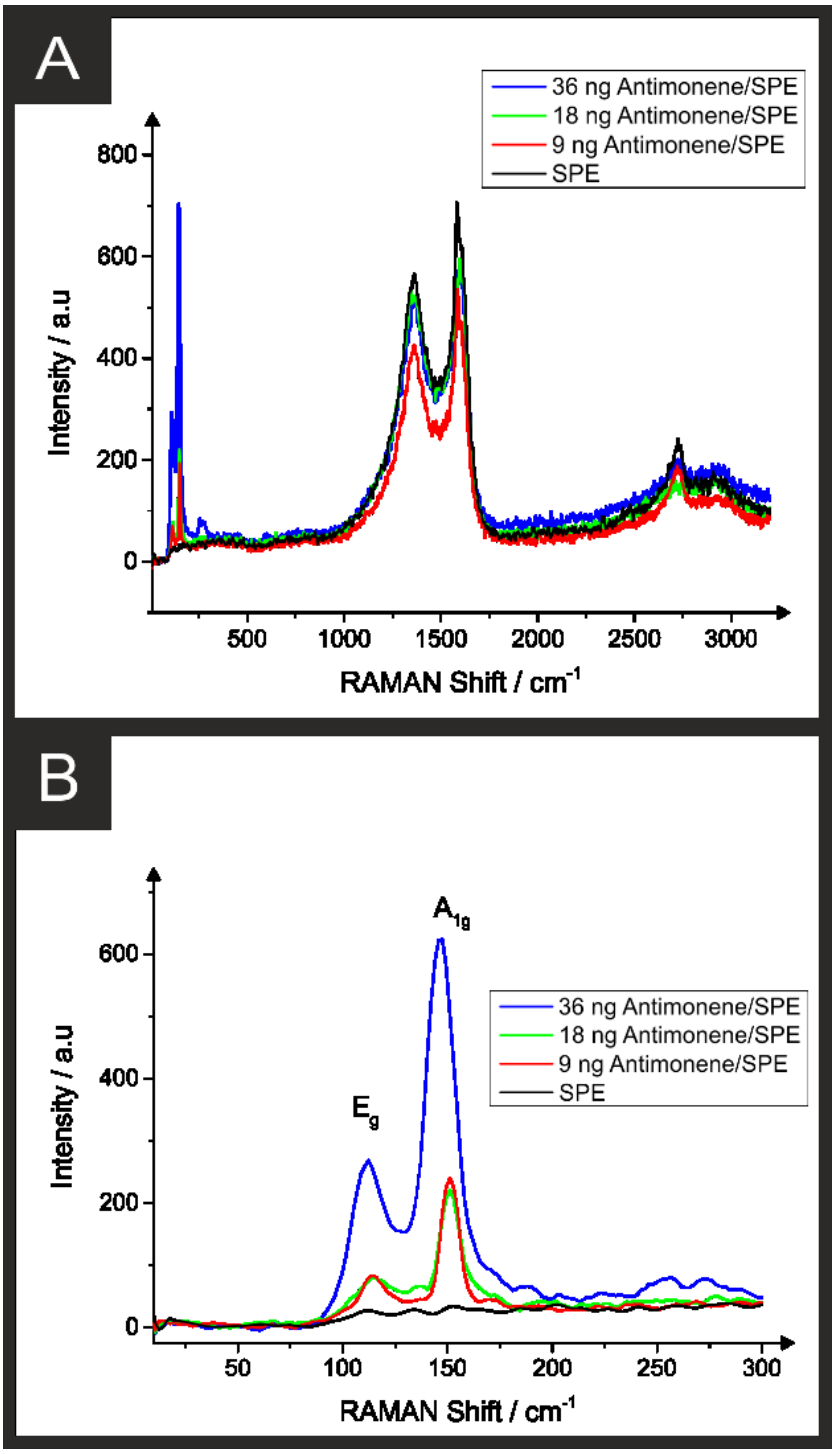

Figure 3-*Cyclic voltammograms obtained with a two electrodes system of SPE and different amounts of antimonene modified SPE at 10 mV/s (A), 100 mV/s (B) and 500 mV/s (C) in 0.5 M H_2SO_4. It becomes clear that the integral area of the CVs, a property that is indicative of the capacitance of the system, is directly proportional to the quantity of antimonene present on the electrode.*

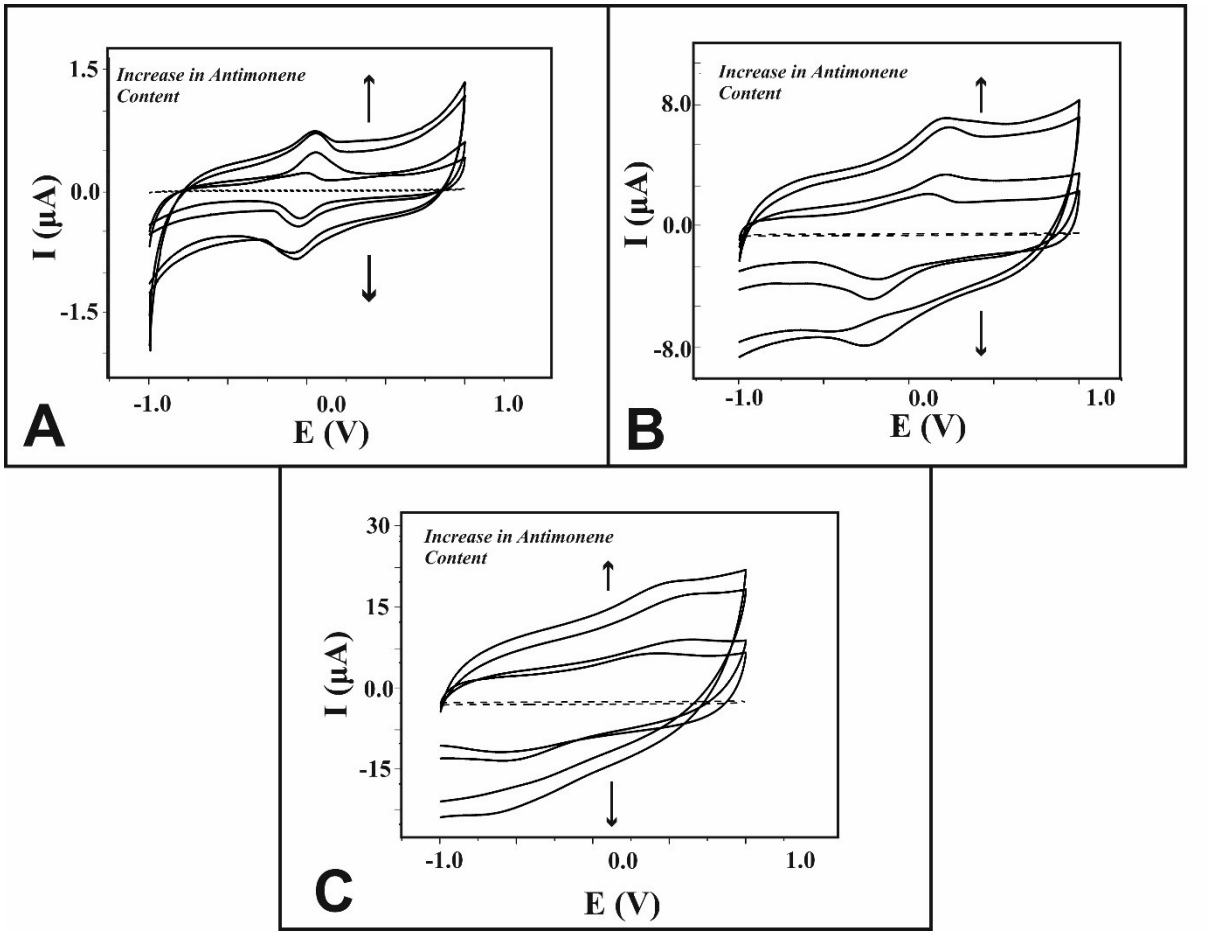

Figure 4. *(A) Charge/discharge profiles recorded in 0.5 M H_2SO_4 with unmodified (black) 1.8 ng (red), 3.6 ng (green), 9.0 ng (blue), 18.0 ng (cyan) and 36.0 ng (pink) antimonene modified SPEs applying 0.05 μA. (B) Capacitances values vs. current applied obtained from charge-discharge profiles. (C) Specific capacitances values vs. specific current applied obtained from charge-discharge profiles. (D) Relative capacitance for successive charge-discharge cycles respect the 1st cycle capacitance. The capacitance of the bare SPE, on it's first cycle, is also indicated. It is shown that the Antimonene enhanced electrodes are consistently performing higher than the bare SPE.*

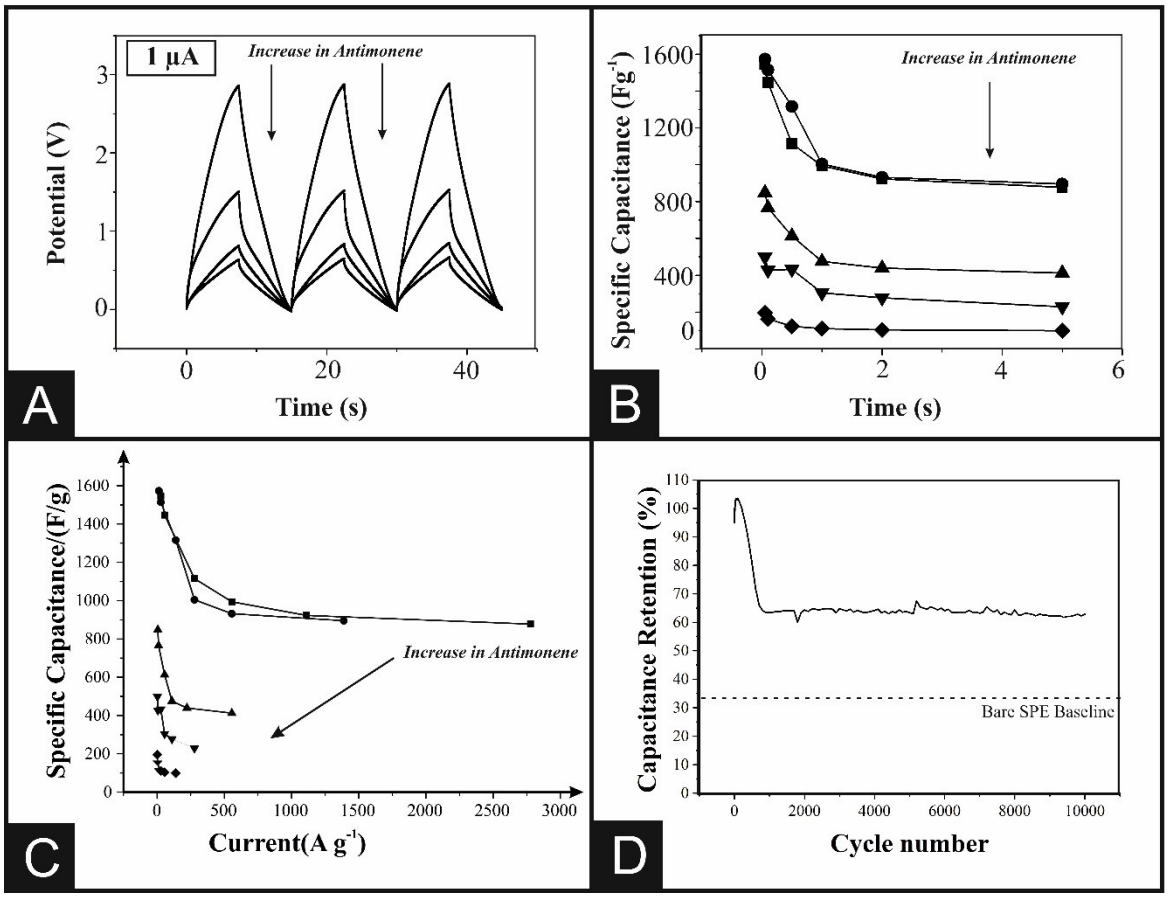

Figure 5. Ragone plot showing the results obtained for Antimonene/SPE and some actual data obtained at bibliography of 2d-nanomaterial or modified 2d nanomaterials. [40,41,48-56] The antimonene supercapacitor, shown as black squares, is compared to: 1) a graphene/sodium cholate enhanced electrode;[49] 2) reduced graphene oxide *paper* electrodes;[48] 3) 2D nanosheets d-MnO_2 / graphene electrodes;[51] 4) Nitrogen crumpled graphene sheets;[52] 5) Nitrogen enriched carbon nanosheets;[53] 6) RuO2/graphene hybrid material;[54] 7) Nickel cobalt sulfide nanosheets;[55] and 8) 2-D titanium carbide.[56]

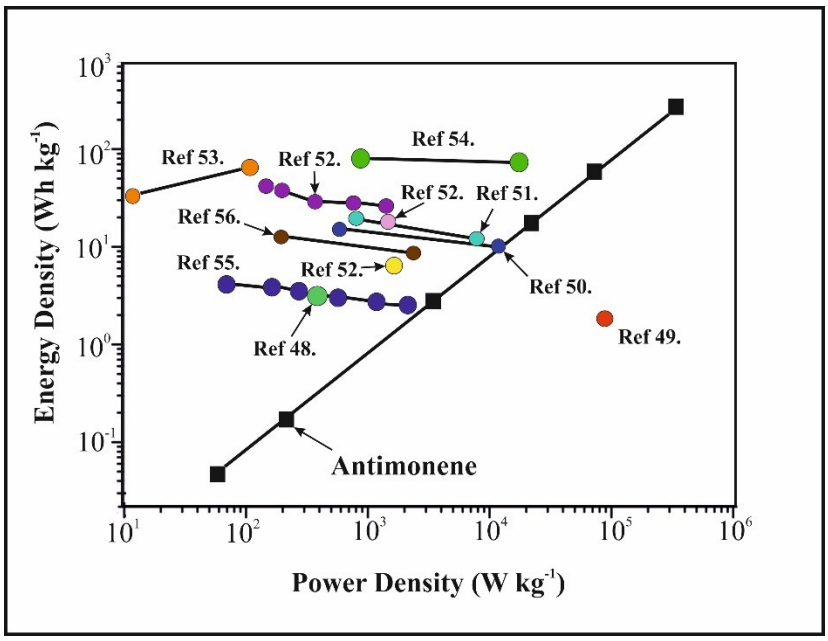

Table 1. *Capacitances values obtained from charge-discharge profiles for different amounts antimonene modified SPEs at different currents in μF.*

	Antimonene mass (ng)				
Current (μA)	**1.8**	**3.6**	**9.0**	**18.0**	**36.0**
0.05	2.78	5.66	7.63	8.98	7.05
0.10	2.60	5.45	6.89	7.69	5.88
0.50	2.01	4.74	5.52	7.79	4.43
1.00	1.79	3.62	4.27	5.47	3.99
2.00	1.66	3.36	3.95	4.99	3.74
5.00	1.58	3.22	3.71	4.12	3.58

Electronic Supporting Information (ESI) for the following publication:

Antimonene: a novel 2d-nanomaterial for supercapacitors applications.

Emiliano Martínez-Periñán,[a, b] Michael P. Down,[b] Carlos Gibaja,[c] Encarnación Lorenzo,[a] Félix Zamora,[c] and Craig E. Banks[b*]

[a]: *Departamento de Química Analítica y Análisis Instrumental, Universidad Autónoma de Madrid, 28049, Madrid, Spain.*

[b]: *Faculty of Science and Engineering, Manchester Metropolitan University, Chester Street, Manchester M1 5GD, UK.*

[c]: *Departamento de Química Inorgánica, Universidad Autónoma de Madrid, 28049, Madrid, Spain.*

*To whom correspondence should be addressed.

Email: c.banks@mmu.ac.uk; Tel: ++(0)1612471196; Fax: ++(0)1612476831

Website: www.craigbanksresearch.com

Table S1. Weight and atomic percentages obtained by EDX of 36 ng antimonene/SPE surface.

Element	Wt%	At%
CK	84.41	90.01
OK	11.89	09.52
SbL	03.69	00.48
Matrix	Correction	ZAF

Table S2. *Specific capacitance values (F/g) obtained from charge-discharge profiles for different amounts antimonene modified SPEs at different specific currents (A/g).*

1.8 ng Antimonene		**3.6 ng Antimonene**		**9.0 ng Antimonene**		**18.0 ng Antimonene**		**36.0 ng Antimonene**	
I (Ag^{-1})	**C (Fg^{-1})**	**I (Ag^{-1})**	**C (Fg^{-1})**	**I (Ag^{-1})**	**C (Fg^{-1})**	**I (Ag^{-1})**	**C (Fg^{-1})**	**I (Ag^{-1})**	**C (Fg^{-1})**
28	1547	14	1573	6	848	3	499	1	196
56	1446	28	1514	11	765	6	427	3	163
278	1115	139	1316	56	613	28	433	14	123
556	994	278	1005	111	475	56	304	28	111
1111	923	556	932	222	439	111	277	56	104
2778	878	1389	895	556	413	278	229	139	99

Table S3. *Specific capacitance values (F/g) obtained from charge-discharge profiles for different amounts antimonene modified SPEs at different specific currents (A/g).*

1.8 ng Antimonene		**3.6 ng Antimonene**		**9.0 ng Antimonene**		**18.0 ng Antimonene**		**36.0 ng Antimonene**	
I (Ag^{-1})	**C (Fg^{-1})**	**I (Ag^{-1})**	**C (Fg^{-1})**	**I (Ag^{-1})**	**C (Fg^{-1})**	**I (Ag^{-1})**	**C (Fg^{-1})**	**I (Ag^{-1})**	**C (Fg^{-1})**
28	1547	14	1573	6	848	3	499	1	196
56	1446	28	1514	11	765	6	427	3	163
278	1115	139	1316	56	613	28	433	14	123
556	994	278	1005	111	475	56	304	28	111
1111	923	556	932	222	439	111	277	56	104
2778	878	1389	895	556	413	278	229	139	99

Table S4. *Specific capacitance data at F/g obtained during CVs measurements using different amounts of antimonene modified SPE at different scan rates.*

	Antimonene mass (ng)				
Scan rate (V/s)/	**1.8**	**3.6**	**9.0**	**18.0**	**36.0**
0.025	8549	6747	2816	2789	1587
0.050	8361	6091	2679	2536	1442
0.075	8246	5790	2537	2365	1347
0.100	8187	5609	2428	2249	1277
0.250	7975	5075	2113	1909	1102
0.500	7538	4498	1843	1617	957

Table S5. Effective heterogeneous electron transfer rate constant, k^{o}_{eff} of bare SPE and modified antimonene/SPE in 1 mM $Ru(NH_3)_6^{3+}$ 0.1 M KCl.

Electrode	**k^{0}_{eff}/ cm·s^{-1}**
SPE	$2.05 \cdot 10^{-3}$
1.8 ng Antimonene/SPE	$2.16 \cdot 10^{-3}$
3.6 ng Antimonene/SPE	$2.23 \cdot 10^{-3}$
9 ng Antimonene/SPE	$2.26 \cdot 10^{-3}$
18 ng Antimonene/SPE	$2.23 \cdot 10^{-3}$
36 ng Antimonene/SPE	$2.09 \cdot 10^{-3}$
72 ng Antimonene/SPE	$2.08 \cdot 10^{-3}$

Figure S1. EDX spectra obtained of 36 ng antimonene/SPE surface.

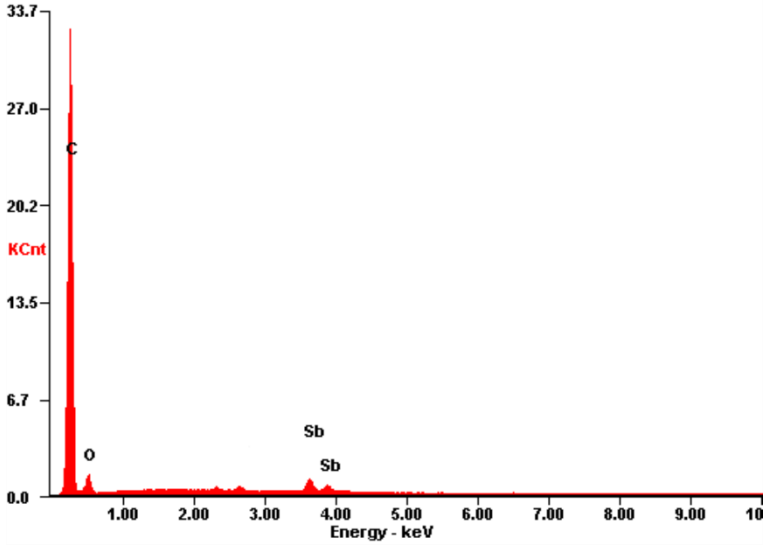

Figure S2. Cyclic Voltammograms of bare SPE (black), 36 ng Antimonene/SPE (red) and 72 ng Antimonene/SPE (green) at 10 mV/s (A), 100 mV/s (B) and 500 mV/s (C) in 1 mM $Ru(NH_3)_6^{3+}$ 0.1 M KCl.

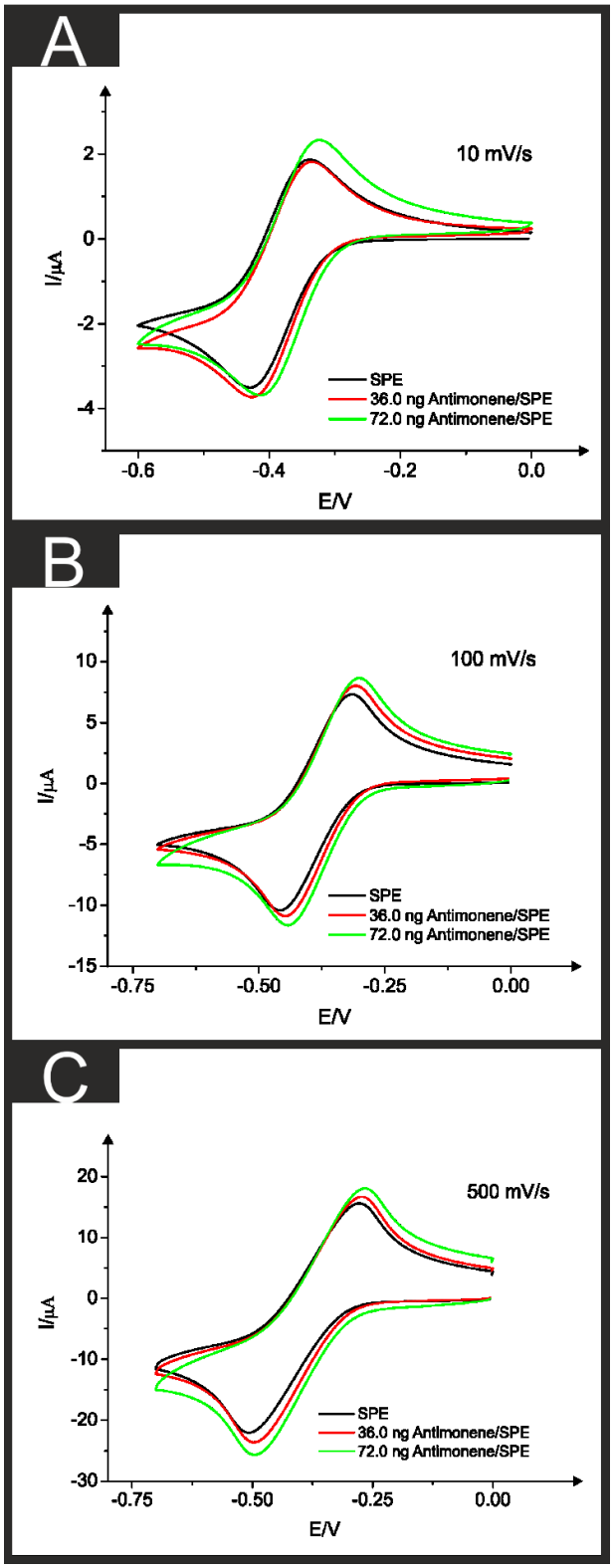

Figure S3. (A) Cyclic voltammograms of bare SPE (red) and 36 ng antimonene/SPE (black). (B) Successive cyclic voltammograms of 36 ng antimonene/SPE. In both cases CVs were obtained at 0.5 M H_2SO_4 using a three electrodes system.